Renewable Energy 237 (2024) 121671

Contents lists available at ScienceDirect

Renewable Energy

journal homepage: www.elsevier.com/locate/renene

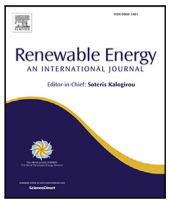

Investigation of wind farm impacts on surface waves using coupled numerical simulations ☆

Xiaoli Guo Larsén [a,*], Jana Fischereit [a], Sima Hamzeloo [a], Konrad Bärfuss [b], Astrid Lampert [b]

[a] Department of Wind and Energy Systems, Technical University of Denmark, Frederiksborgvej 399, Roskilde, 4000, Denmark
[b] Institute of Flight Guidance, Technische Universität Braunschweig, Braunschweig, 38108, Germany

ARTICLE INFO

Dataset link: https://doi.pangaea.de/10.1594/PANGAEA.902845

Keywords:
Wind farm parameterization
Wind farm effect
Wake
Wave modeling
Sea state
WRF
SWAN
SDG7

ABSTRACT

A numerical investigation is carried out to understand the effect of offshore wind farm wakes on the surface wind and hence water waves. Two cases with the presence of wind farm wake effects from the literature are revisited, mainly due to two reasons: (1) the availability of various atmospheric and wave measurements; (2) one case with fetch effect and one without fetch effect. The coupled modeling system includes the atmospheric model WRF and ocean wave model SWAN, with the Wave Boundary Layer model implemented in SWAN. The wind farm wake effects are modeled using the Fitch Wind Farm Parameterization, where we used four coefficients of the parameter α to adjust the turbulent kinetic energy (TKE) coefficient (relevant to the magnitude and hence indirect advection of turbine-generated TKE: $\alpha = 1$, 0.25, 0.1 and 0). For the two cases, measurements suggest reduced wind speed and wave height under the wind farm wake effect. The modeling results are consistent, except for when $\alpha = 1$ is used. Using the currently standard value of $\alpha = 1$ results in excessive turbine-generated turbulence transported to the surface. This leads to enhanced surface winds and wave height; as this contradicts the measurements, we conclude that it is a numerical artifact. The study points to the importance of future research on a more accurate description of the horizontal and vertical transport of the turbine-generated TKE in WRF.

1. Introduction

Offshore wind energy development has never been so rapid, and the sizes of wind farm clusters can be as large as several hundreds kilometers by several hundreds kilometers. The presence of these large-scale wind farms affects not only the atmosphere, but also surface water waves. There have been increasing number of studies on the interaction between atmosphere and turbines/wind farms; the studies on the interaction between atmosphere, turbines/wind farms and surface water waves are few.

In the presence of wind farms, around the turbine hub height, wind speed is reduced inside as well as downwind of the wind farm, as a result of wake effects. Intuitively, it is expected that the wake effects originated from the height of the rotor blades propagate both horizontally and vertically, and consequently, wind speed in the atmospheric surface layer, defined here as the lowermost altitude from the surface up to about 10 m may also be reduced. The reduced surface winds, when over water surface, suggest weaker drives to the generation of water waves, compared to no-wind-farm (NWF) conditions.

While most studies using satellite based data of Synthetic Aperture Radar (SAR) for wind farm wake investigations suggest a reduced wind speed at 10 m altitude downwind of the farms, Djath et al. [1] and Hasager et al. [2] observed some cases with enhanced scatter signals in the SAR images and interpreted these signals as air flow "acceleration". Enhanced turbulence is another feature associated with wind farm and wind turbine wake effects. The "acceleration" signals were sometimes interpreted as high turbulence, which the SAR algorithms translate into enhanced wind speed.

The acceleration effect has also been reported in mesoscale simulations of wind farm wake effect in association with the Fitch Wind Farm Parameterization (WFP) in the Weather Research and Forecasting (WRF) model [3]. The Fitch WFP adds a sink term $\overline{f}_t$ to the momentum equation in WRF

$$\overline{f}_t = \frac{1}{2} C_T U^2 A_r / \Delta \forall. \quad (1)$$

where C_T is the thrust coefficient, U is the wind speed in the grid cell, A_r is the rotor area and $\forall$ V a control volume. Further the Fitch WFP

☆ This study was supported by the DFF MAMAS project (nr. 0217-00055B), Danish EUDP project GASPOC (J. nr. 65020-1043), EU Horizon project DTWO (J. nr. 101146689).

* Corresponding author.
E-mail address: xgal@dtu.dk (X.G. Larsén).

https://doi.org/10.1016/j.renene.2024.121671
Received 4 July 2024; Received in revised form 8 October 2024; Accepted 21 October 2024
Available online 28 October 2024

scheme adds a source term to the Turbulence Kinetic Energy (TKE) equation

$$\overline{p}_t = \frac{1}{2}\alpha(C_T - C_P)U^3 A_r, \quad (2)$$

Here, C_P is the power coefficient. The original paper of WFP, Fitch et al. [3] effectively uses $\alpha = 1$ in Eq. (2). To explain their simulation of enhanced wind speed at the surface as a result of wake effect, [3] showed the vertical distribution of the momentum flux $\overline{u'w'}$, with the values of $\overline{u'w'}$ at the surface being positive. This was considered as a result from a possible excessive momentum, generated at the hub height and transported to the surface. The positive surface momentum flux $\overline{u'w'}$ contributes to an increase in wind speed there. When using the model for the added TKE from turbines from Fitch et al. [3], Larsén and Fischereit [4] (hereinafter LF2021) also simulated the acceleration of the wind speed at lowest levels.

Fitch et al. [3] calculated TKE from the MYNN2 PBL scheme in WRF. In this scheme, TKE is predicted in each vertical column separately, through a one-dimensional TKE equation, which depends only on the vertical coordinate. Archer et al. [5] re-introduced the scalar array called QKE_ADV to ensure that turbine-generated TKE is treated as a scalar, whose advection can be calculated the same way as other scalars. In addition, Archer et al. [5] provided the coefficient α to be used in connection with the TKE coefficient $C_{TKE} = C_T - C_P$, as shown by Eq. (2). Archer et al. [5] used $\alpha \cdot C_{TKE}$ to adjust the magnitude of turbine-induced TKE as in the Fitch WFP. They found an "optimal" value of α as 0.25, based on their comparisons of a single turbine with Large Eddy Simulations (LES).

LF2021 tested the adjusted TKE following Archer et al. [5] and found that using $\alpha = 1$ provides best agreement of wind statistics at hub height between simulation and measurements for studied offshore wind farms, and at the same time, the acceleration of surface winds in the wake area only occurred when $\alpha = 1$, but not when $\alpha = 0.25$. Bodini et al. [6] also found from their WRF modeling of onshore wind farms that "...near the surface, accelerations occur in stably stratified conditions but only for the simulations with 100% TKE included (i.e. $\alpha = 1$)". Using a different wind farm parameterization from the Fitch scheme, the explicit wind farm parameterization (EWP) used in WRF, Volker et al. [7] did not find the corresponding acceleration in connection with the wakes for idealized simulations. The EWP scheme does not include the extra term (Eq. (2)) in the TKE equation, and only adds wake-induced TKE from the wake-affected wind profile, e.g. through shear. Previous studies consistently suggest that, while EWP provides reasonable wind speed reduction, its TKE is significantly underestimated. When using EWP, LF2021 neither got surface wind acceleration in their real case simulation. The LES simulation of wind farm effects from Wu and Porté-Agel [8] (their Fig. 13) neither supported the surface flow acceleration. Such an acceleration was however present in the LES results by Vanderwende et al. [9] for stable conditions.

The effect of wind farms on the wave field has only been addressed by very few studies. Fischereit et al. [10] applied $\alpha = 0.25$ to model a 30-year worth statistics of wind and wave fields in the presence of wind farms in the German Bight, and found reduced long-term significant wave height H_S in areas around the wind farms. Porchetta et al. [11] also studied the wave fields under the impact of wind farm wakes in the German Bight using the COAWST system with a roughness length parameterization scheme for the surface waves from Porchetta et al. [12]. Studies using measurements on this subject are even fewer. Platis et al. [13] reported on enhanced surface reflectance of a laser scanner within the wind farm wake, which is interpreted as smoother surface compared to the areas not influenced by wakes. Wave height in the vicinity of wind farms (1 km downwind of the wind farm) have been measured using airborne laser scanner [14], and Dörenkämper [15] reported, from an unpublished data analysis, reduced significant wave height (H_S) in the wake area. Bärfuss et al. [16], called B2021 hereinafter, analyzed the measured wave spectra inside and outside the wind farm wake regions, with winds from land over the offshore wind farms (their Fig. 4). They found that the spectral wave energy is considerably smaller in the wake region than outside of it, though they also observe increasing wind speed in the background from the Danish coastline over to the open water in the North Sea.

The literature has provided very few and scattered puzzle pieces of the atmosphere close to water surface in the presence of interaction of atmosphere, wakes and waves. Particularly, relevant researches are severely limited by lack of measurements to verify hypotheses and modeling. This study serves as one of the unfolding investigations, and here we revisit two published studies on this subject where measurements were used. At the same time, we strengthen the existing investigations by introducing numerical modeling that include atmosphere, waves and wind farm wakes. We experiment with the measurements-modeling combined approach, aiming at obtaining better understanding of the observations where the signals of wind farm wake impacts are sometimes difficult to read. Thus, we gain insights to the several research questions, including: How is modeling of the wave field affected by the use of WFP scheme? How does the distribution of turbine-generated TKE from hub height to surface affect the wave field? Can the surface wind speed and waves be enhanced as a result of the wind farm wake effect?

The detailed method is introduced in Section 2, followed by results in Section 3, discussions in Section 4 and conclusions in Section 5.

2. Method

In this study we use case studies. Case studies are limited in providing answers to general questions. They are nevertheless good to start a systematic investigation, here particularly on testing the method of the atmosphere-wave-wind farm coupled modeling, to help us get insight of background mechanisms of air–sea-wake interaction.

As there are very few studies on this research subject involving measurements, we identified two cases: Case-1 from B2021 and Case-2 from LF2021, and continue these investigations by adding new elements to their methods.

Besides that there are measurements available, these two cases also complement each other on the wind farm cluster situation in relation to upwind land. They thus bring different levels of challenges and opportunities to the investigations. Specifically, Case-1 is chosen here because B2021 published the wave spectra and wave height in tracks up- and downwind of the wind farms with systematic flights deploying an airborne laser scanner during the day on 8 August 2017 (2017-08-08). Case-1 is, however, complicated by the presence of both fetch and wind farm effects. On this day, the winds were from land over water. We continue B2021's study by adding the numerical simulation to the data analysis. Case-2 is chosen here because LF2021 demonstrated successful numerical simulation of wind farm wakes, validated by SAR, mast measurements from FINO 1 and flight data. We continue LF2021's study by extending the simulation with a wave model coupled to WRF (see Section 2.2). In contrast to Case-1, Case-2 has a negligible fetch effect.

Table 1 lists some basic information of the two cases, including dates, flow conditions, flight heights, and respective wind farm clusters and the hub height.

2.1. Cases and measurements

Case-1 involves the wind farm cluster including, from the north to the south, Amrumbank West, Kaskasi gap, Nordsee Ost and Meerwind Süd/Ost, which is called wind farm cluster N4 in B2021 and we adopt N4 here (Fig. 1). The flight legs can be found in B2021, and the atmospheric data are published in Bärfuss et al. [17] and described in Lampert et al. [18]. The transects where data are recorded are reproduced here in Fig. 1, labeled with flight leg numbers. There are altogether 10 transects, with Flight Leg numbers 1 to 10; with winds from land to sea, Flight Leg 1 is thus upwind of N4. Sometimes there

Table 1
Overview of the two selected cases in this study. 'wf': wind farms; 'hh': hub height; 'mh': measurement height. The locations of the wind farm clusters N3 and N4 are indicated in Fig. 1.

	Day	Wind direction	Fetch	wf	hh (m)	mh (m)	Ref.s
Case-1	2017–08–08	East	short	N4	90 m	91 m	B2021
Case-2	2017–10–14	West-Southwest	long	N3	120 m	120 m	LF2021

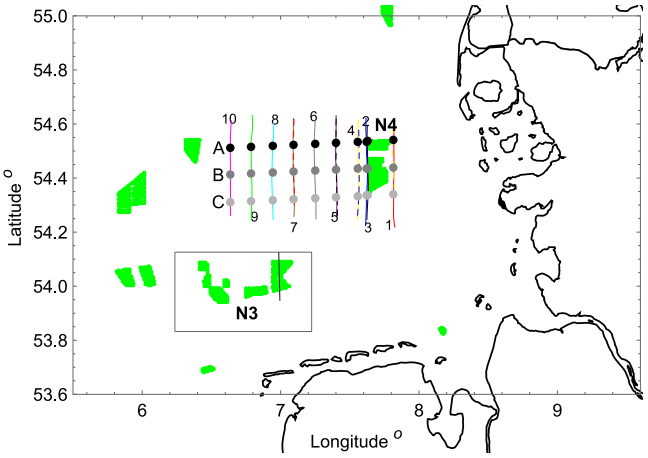

Fig. 1. Case-1. Flight legs shown in different colors, labeled with numbers 1 to 10. Also shown are three rows of dots, with the black (A) and dark gray (B) ones in the wakes of N4 (except two upwind of the farms), and the light gray ones (C) outside the wakes. The wind cluster N3 is marked with a box, with the black line across the Godewind1 being the transect with flight data analyzed. Note that N4 is relevant for Case-1 and N3 is for Case-2. The green dots represent individual wind turbines, which are clustered in wind parks.

is more than one flight along one transect, e.g., Flight Leg 2 and 3 are almost on the same transect, but were flown in opposite direction.

B2021 presented the distribution of wind speed and spectral wave energy along the flight legs in their Fig. 3, which is reproduced here as a part of Fig. 2. In addition, we added the data from transects with shorter distances to the farm cluster N4 at 2 km, 5 km and 15 km (Flight Leg 2-5), in order to examine in more details the flow in the vicinity of the wind farms.

For Case-1, with the wind direction from the east, the atmospheric flow is advected from land over water, and reached wind farm cluster N4 with limited fetch. Under the fetch effect, it is expected that wind speed and consequently, wave energy will increase (Section 3.2). Such an effect counteracts the wake effect. Thus, for Case-1, the area around N4 (Fig. 1) is influenced by the wind farm wake and the offshore fetch effects. Fig. 2 confirms the above arguments; the corresponding wind and wave fields are characterized by (1) increased fluctuations in wind speed at hub height in the wakes, and the fluctuations decrease with distance away from the wind farm (2) clearly reduced wind speed at hub height corresponding to the farm Amrumbank West, and accordingly weakened wave energy (3) overall wind speed increase and wave energy with increasing fetch distance to the shore. On the day of Case-1, the SAR data are only available mostly outside our study area, see Fischereit et al. [19], and it is therefore not shown here. The SAR image also shows a large spatial variation of weather patterns over the North Sea, corresponding to highly varying wind conditions over the region.

Case-2 was modeled and validated in LF2021 using WRF without coupling to a wave model. The relevant wind farms for Case-2 were referred to as "N3" in the studies of WIPAFF and X-Wakes (e.g., Dörenkämper [15]), we also call this cluster N3 here (Fig. 1). Even though no laser scanner data of the surface is available for Case-2, the simulations of the wind field have been shown to be reliable through validation using mast (FINO 1, time series and wind profile), SAR and flight measurements in LF2021. Case-2 thus provides an opportunity to examine the wave field without interference of fetch effect.

2.2. Modeling

We use DTU's coupled modeling system, which is based on the Coupled-Ocean-Atmosphere-Wave-Sediment Transport model (COAWST version 3.2, 20). It includes WRF version 3.7.1, 21, the Spectral WAve model Nearshore (SWAN version 41.01, 22) and the wave boundary layer model (WBLM) implemented in SWAN as developed in Du et al. [23] and updated in Du et al. [24]. We employ the same three one-way nested domains with 18 km, 6 km and 2 km resolution for both WRF and SWAN. The model domain for Case-1 centers around wind farm cluster N4 and is shown in Fig. 3, the domain for Case-2 can be found in LF2021 (their Fig. 4) with Godewind1 and surrounding farms in the model center, where the flight data are available.

WRF and SWAN are two-way online coupled through the WBLM. The WBLM solves the height-dependent equation for the total stress, consisting of turbulent and wave-induced stress. Furthermore, the WBLM solves the conservation equation for the kinetic energy with height, thereby ensuring that the momentum transfer between wind and waves is both flux and energy consistent. To do so, WRF sends the horizontal 10-m-wind components to SWAN and in return receives a corresponding roughness-related length which is a function of wave-induced stress. The details can be found in Du et al. [24]. The exchange frequency between WRF and SWAN is once per 6 minutes. The simulation length is 24 h with a 6-hour spin-up time. The time step for the WRF outer domain is 45 s, and the time step for SWAN is 6 min. The model outputs are saved every 10 min. More details on the set-up, including the used parameterizations, boundary and initial conditions are given in Table 2.

Compared to measurements, an obvious strength of using modeling is that we can activate or deactivate wind farm effects, in the presence of the fetch effect, by activating and deactivating the WFP schemes. Different WFP have been developed in the past and a comprehensive overview can be found in Fischereit et al. [25].

Here we use the Fitch WFP scheme [3], which is included in the official WRF model. The corresponding sink term to the momentum equation and source term to the TKE equation by the Fitch WFP are presented in Eqs. (1) and (2).

We incorporated the updates by Archer et al. [5] to ensure the proper advection of turbine-induced TKE. The coefficient α in Eq. (2) adjusts the amount of turbine-induced TKE. For small values of α, turbine induced TKE is small. However, ambient TKE is still evolving due to advection, shear, buoyancy, turbulence transport, pressure correlation and dissipation of the ambient flow. As highlighted in Introduction, the "best" value for α is not yet known, thus we test four values α = 1, 0.25, 0.1 and 0 in this study and examine the corresponding impact on the wind speed at the lowest model level of 10 m and accordingly the impact on the waves. α = 1 was initially used in the original WFP paper by Fitch et al. [3], and it is used here to examine the maximum effect of turbine-induced TKE. This value has been frequently used, including recent studies, e.g., [26,27]. α = 0.25 was chosen as a reference, since it is the recommended value based on Archer et al. [5], who determined it based on LES simulations with a single turbine. α = 0 is chosen to examine the extreme effect of not including any turbine-induced TKE; this configuration is most similar to the assumption of the EWP scheme [7], another frequently used WFP. The value of α = 0.1 has been chosen as an additional numerical test to have a value between α = 0 and 0.25.

The long-fetch Case-2 was run in LF2021 using WRF only, where α = 1 and 0.25 were used. Here the case was re-run using the coupled modeling system, using four α values the same way as for Case-1.

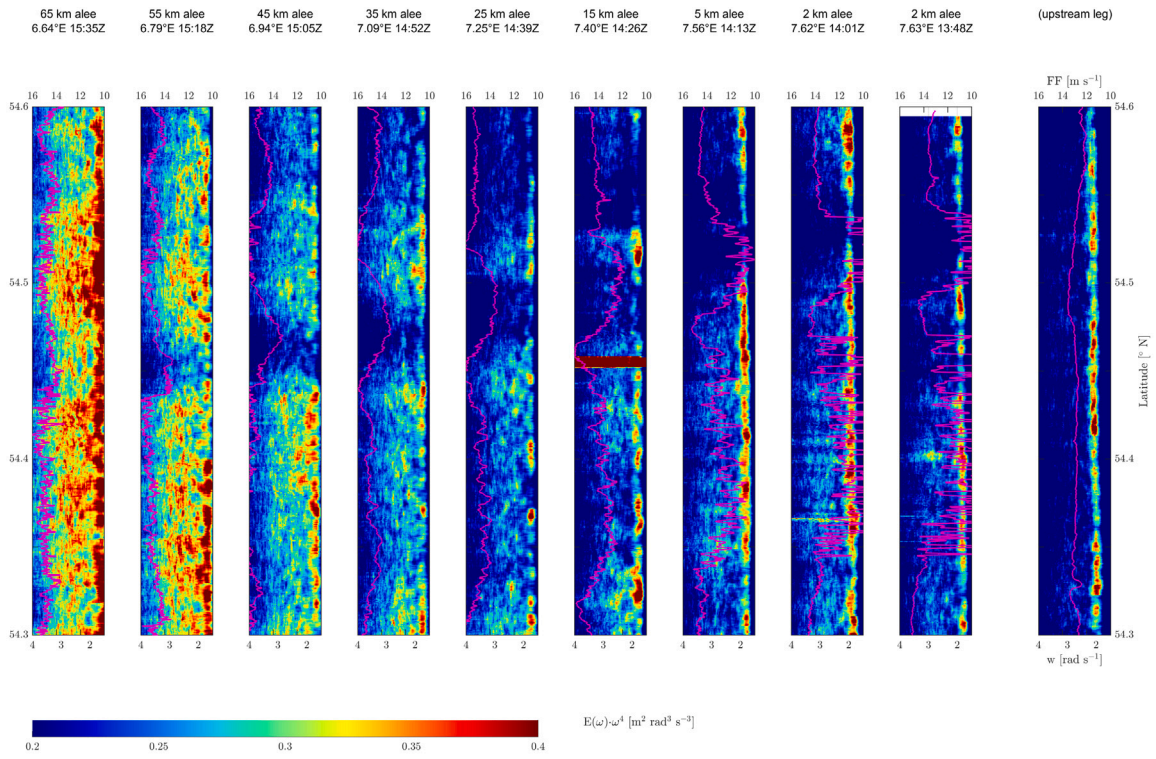

Fig. 2. Case-1. 10 flight legs with wind speed measured around hub height (lines in magenta), and sea surface energy distribution, along the flight leg upstream (the one to the right) and downstream of the wind farm cluster N4 on 8 August 2017. The transects with distance from N4 at 65, 55, 45, 35, 25 km and upstream leg are reproduced from B2021.

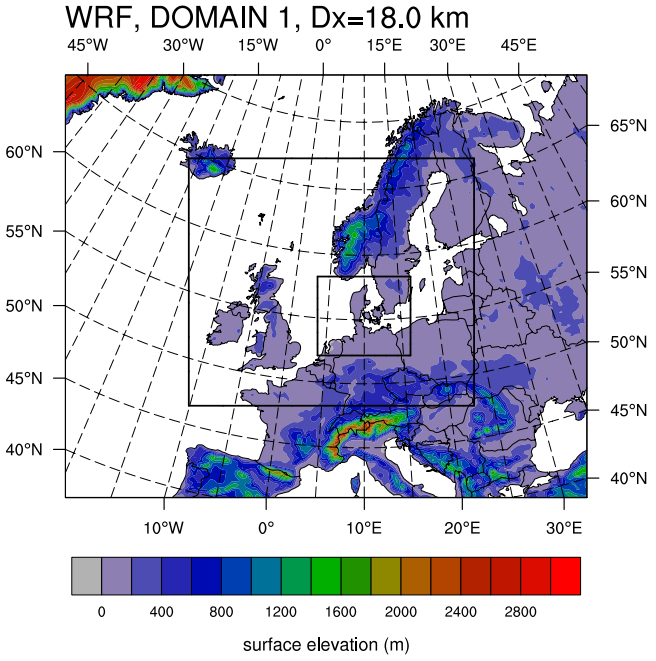

Fig. 3. The three nested WRF model domains shown in surface elevation for Case-1 on 8 August 2017.

The wind farm and turbines information used in WRF for the simulation is obtained from LF2021 (see Table 4 in LF2021).

To understand the wake effect, the following variables are analyzed: (1) Wind speed at lowest model level over the wind farm area (2) Vertical wind speed profile over the wind farm and in the wake region (3) Significant wave height H_s over the wind farm area and in the wake region (4) Wave spectra upwind, and inside of the farm and in the wake region.

3. Results and analysis

3.1. B2021: Wake effect or spatial variability?

B2021 presented their measurements of the wind speed at an altitude of 91 m (approximately the hub height) and wave spectra along the flight legs during two hours between about 13:30 UTC and 15:35 UTC on 8 August 2017, over, upwind and downwind of N4. The modeled wind speeds at around 91 m, U_{HH}, along the corresponding flight legs and timing as in Fig. 2 are shown in Fig. 4a, for no-wind-farms (NWF), as well as with wind farms (with $\alpha = 1$, 0.25, 0.1 and 0), respectively. The corresponding wind speed deficit at 90 m (ΔU_{HH}) between WFP and NWF is shown in Fig. 4b. One can see that for Flight Leg 1, upwind the wind farm, the wind speeds from the five simulations are very close, showing a very small blockage effect. The modeled wind speed shows similar pattern along the flight leg to the measurements (see Fig. 2, the magenta line on the right-most panel), and the wind speed at 90 m is between 10–12 m s^{-1}, slightly lower than the measured values. Downwind of N4, both measurements (Fig. 2) and modeling show that the mean wind speed increases, most likely as a result of increasing fetch effect. The fetch effect will be discussed in more details in Section 3.2. At the same time, a significant deficit in the wind velocity U_{HH} (WFP minus NWF) appears in the vicinity of N4 downwind, and the magnitude of the deficit reduces with distance from the wind farm, suggesting a weakened wake effect, which becomes negligible at a distance of about 55 km (Flight Leg 9). The distance where the wake effect becomes negligible varies with height, see the analysis over the longitude-height transects in Section 3.4.

The wake effect reflected in the modeled TKE at 90 m, TKE_{HH}, did not extend as far as for wind speed, and seemed to be negligible at a distance of 15–25 km. The extension of wake effect on TKE at hub height is comparable to the study of the same case using both the

Table 2
Set-up of the WRF and the SWAN models in the coupled modeling system.

Category	Model	Subcategory	Details (WRF option number)
Time	Simulation length		24 h, 6 h spin-up
	Output time step		10 min
	WRF	time step	45 s
	SWAN	time step	6 min
	Coupling	exchange time step	6 min
Resolution	WRF, SWAN	horizontally	18 km, 6 km, 2 km
	WRF	vertically	80 sigma levels up to a model top of 50 hPa with 24 (mass) levels in the lowest 250 m, i.e. about 10 m spacing in the lowest levels
	SWAN	frequency	61 frequencies between 0.03 Hz and 10.05 Hz with a frequency exponent of 1.1
		direction	36 bins
Boundary, Forcing	WRF	dynamical forcing data	ERA5
		land use data	CORINE
		sea surface temperature	OSTIA
		land surface model	NOAH-LSM (2)
	SWAN	bathymetry	1/8 arc-minute bathymetry data from EMODnet Digital Terrain Model (DTM)
		boundaries	Open boundaries of outer domain set to zero
		initial conditions	Spectra of a previous uncoupled 24-hour-long SWAN simulation
Schemes	WRF	PBL	MYNN (5)
		Surface layer	MO (2)
		Microphysics	Thompson graupel scheme (8)
		Radiation	RRTMG scheme (4)
		Cumulus parameterization	Kain-Fritsch scheme (1) only in domain 1
		Diffusion	Simple diffusion (1) 2D deformation (4) 6th order positive definite numerical diffusion (2) rates of 0.06, 0.08 and 0.1 for domain 1, domain 2 and domain 3 vertical damping.
		Advection	Positive definite advection of moisture and scalars (1), activated TKE advection
	SWAN	Wave breaking	Constant, $\alpha = 1.0$ and $\gamma = 0.73$
		Bottom friction	JONSWAP $cf_{jon} = 0.038$

WRF and the mesoscale model HARMONIE in Fischereit et al. [19]. As expected, the simulated TKE_{HH} using the four $\alpha-$ values are almost the same along Flight Leg 1, and in correspondence to the largest wind speed deficit, there is the largest increase in TKE_{HH} along Flight Leg 2 and 3. The enhanced TKE_{HH} as a result of wakes decreased rapidly from the wind farm to 15 km downwind. Compared with U_{HH}, the effect of the different values of α becomes obvious on TKE, both at 90 m and at 10 m. $\alpha = 1$ corresponds to largest turbine-generated TKE_{HH}; accordingly, ΔTKE_{10m} is largest with $\alpha = 1$, which is sometimes even positive, suggesting the presence of excessive TKE, transported from the hub height. The strong correlation of ΔU_{10m} and ΔTKE_{10m} suggests that the acceleration associated with wakes is caused by this excessive turbulence transported from the hub height to the surface under the impact of a large α. The acceleration disappears completely when the enhanced TKE_{HH} becomes negligible at a distance of about 15 km downwind of the farms N4. Further downwind, as shown in Figs. 4 and 5, the differences in both wind speed and TKE, at both 90 m and 10 m, between different α, become negligible.

Compared to wind speed and TKE in the surface layer, the behavior of H_S is similar but slightly different, shown in Fig. 5c. The correlation between H_S and U_{10m} (subplot-a) and TKE_{10m} (subplot-b) is strong. When $\alpha = 1$, the positive ΔTKE_{10m} corresponds to positive ΔU_{10m}, as well as positive ΔH_S. The values of ΔU_{10m}, ΔTKE_{10m} and ΔH_S are mostly negative at $\alpha = 0.25$, 0.1 or 0. Similar to ΔTKE_{10m} and ΔU_{10m}, downwind of the wind farm cluster N4, the deceleration first strengthens and then weakens, with the largest reduction in H_S 25 km downwind of N4 (along Flight Leg 10). While the difference caused by α became negligible for U_{10m} and TKE_{10m} at a downwind distance of 15 km, such effect on H_S continues longer than 25 km. There is a spatial phase shift of the wake effect from hub height to the surface, as will be discussed later in Section 3.3.

Here we use the wave measurements through airborne laser scanner in B2021 for validation. The wake effect on the wave field was assessed in B2021 by comparing wave spectra from two rows of data, with one “in the wakes”, which is close to our transect-B (Fig. 1), and one “outside the wakes”, which is close to the our transect-C in the same figure. We add one more transect-A to the north for the discussion of the spatial variability.

The wave spectra measurements from B2021 are shown here in Fig. 6e, for transect-B (dashed curves) and C (solid curves) for Flight Legs 6–10. The corresponding relative differences between the two transects are shown in Fig. 6f for Flight Legs 6–10 (with the additional Leg 10 compared to B2021). We present the results from modeling in a similar way by displaying the wave spectra from transects “under the wake effect” (A and B) and from transect “outside the wake area” (C), here including both WFP ($\alpha = 0.25$) and NWF. Similar to Fig. 6e, Fig. 6a show the simulated wave spectra in the absence of wind farms, from Flight Leg 5 (15 km from N4) to 10 (65 km from N4), following

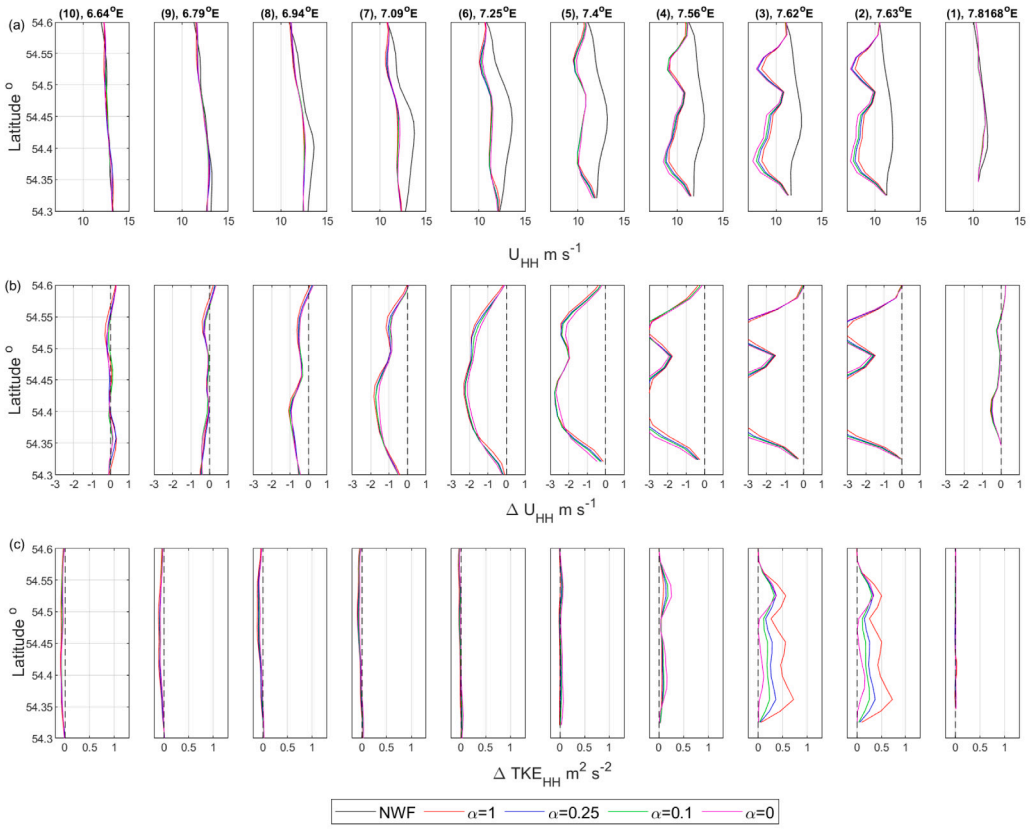

Fig. 4. Case-1. Transects along the 10 flight legs from simulations at hub height. (a) Wind speed at hub height, U_{HH}, without and with WFP where $\alpha = 1$, 0.25, 0.1 and 0 (colors are explained in the legend); (b) Difference in wind speed at hub height, ΔU_{HH}, WFP-NWF; (c) Difference in TKE at hub height, WFP-NWF. The longitude of each flight, and the corresponding flight number are printed in the title of the first row figures. Model data with matching time of the measurements are used.

the three transects A, B and C. Fig. 6c shows such a distribution of wave spectra in the presence of wind farms by using $\alpha = 0.25$ in the Fitch scheme. Fig. 6b (NWF) and d (WFP $\alpha = 0.25$) show the spectral difference in percentage between transect-B and C, corresponding to Fig. 6f.

Conceptually, due to the presence of wind farms, Fig. 6c and d, in the presence of wind farms, are expected to align with the "real situation" Fig. 6e and f. Fig. 6 shows that the model results are consistent with the observations in B2021 on the following aspects: (1) As the distance from N4 and the shore increases, the peak frequency of the wave spectrum decreases and the corresponding spectral energy increases, suggesting longer and higher waves at longer fetch. This is the case for both simulations without (Fig. 6a) and with (Fig. 6c) wind farms. (2) The wave energy "in the wakes" on transect-A and B is lower than that "outside the wakes" on transect-C. This is true, however, for both simulation with and simulation without wind farms. It thus raises the question if the difference between transect-B and C is actually caused by wakes from N4, or by the spatial variability, or both. Comparing the energy level in Fig. 6a and c, it can be observed that the energy level with wind farms (Fig. 6c) is overall lower than that without wind farms (Fig. 6a). (3) the modeled significant reduction in wave energy around the peak frequency is similar to that from measurements, both for NWF and $\alpha = 0.25$, particularly in the frequency range 1–2 rad s^{-1} (cf. Fig. 6b, d and f). The overall wave energy along transect-B is lower than transect-C, which for NWF is less than 10% and for $\alpha = 0.25$, it is less than 20%. Fig. 6b shows the energy difference that is from spatial variability, and not from the wakes of N4, as wind farms are not included in the simulation. The wakes from N4 contributed additionally, with enhanced energy reduction closer to N4, showing a dependence of the downwind distance (Fig. 6d); such a dependence is more obvious in Fig. 6f than in Fig. 6b. Such an effect is most obvious for waves with frequencies larger than the peak frequency, as in Fig. 6d and f, while not so much in Fig. 6b. We note that the calculation of the relative difference is sensitive to the small values of $S(\omega)$ at high ω.

3.2. The fetch effect

It was possible to separate the wake effect from other effects when applying the numerical modeling. The numerical modeling strongly suggests the presence of spatial variability, which further suggests that the measurement data from B2021 are mixed with effects from spatial variability and wind farm wakes from N4.

The spatial variability can result from general mesoscale, weather-related, atmospheric flow in the region. It could also be affected by the fetch effect, as the wind was blowing from land over the sea during this case. For the wind, the fetch is defined as the unobstructed distance that wind can travel over water in a consistent direction. As a result, there is an increase in wind speed as the fetch increases, causing wind gradient from coastline to open water. Fig. 7a shows such wind gradient over the area with lower wind speed closer to land. Fetch is an important factor for wave development; as the fetch increases, waves grow higher and longer. This was already shown in the wave spectra in Fig. 6a, c and e. The growing waves with the fetch are also shown in Fig. 7b in terms of the significant wave height H_S.

This increasing trend in wind speed and wave height as the distance from the shore increases is counteracting with the wake effect in the area downwind of the wind farms. Here, the wake effect causes reduced wind speed, although the reduction weakens with distance from the wind farm. This effect can cause challenges in analyzing the measurements.

It is different for Case-2 from LF2021, for which the wind farm cluster N3 around Godewind1 is studied. The cluster N3 is shown in

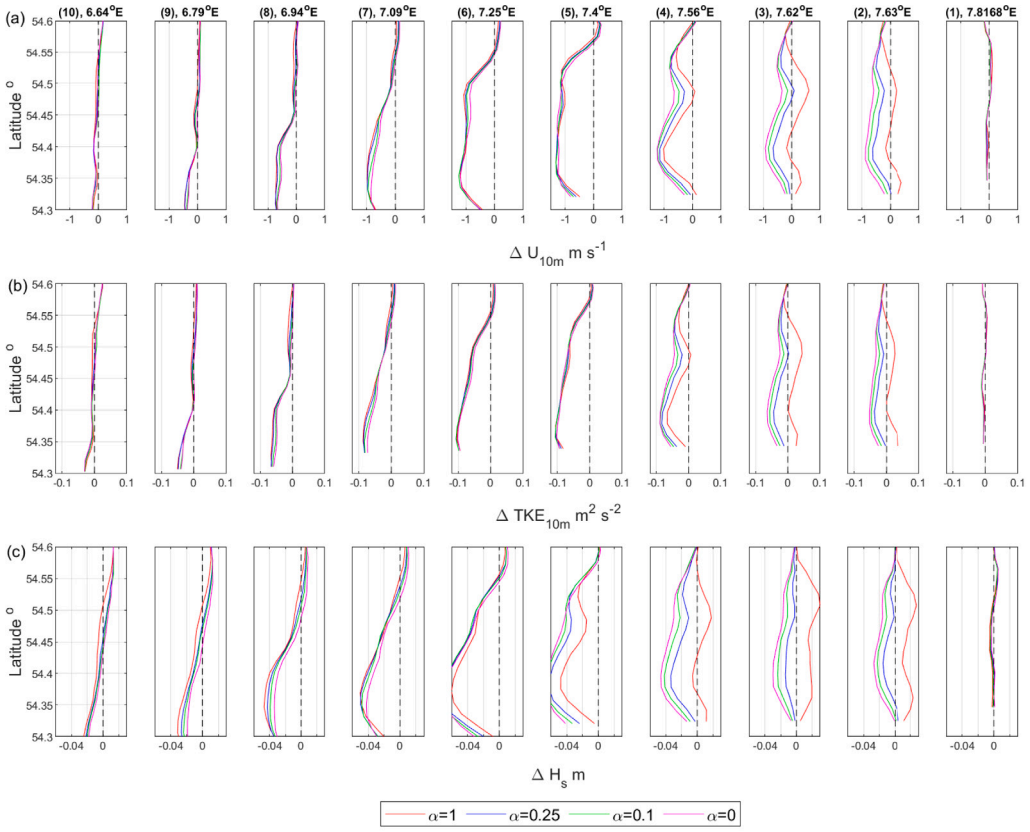

Fig. 5. Case-1. Transects along the 10 flight legs from simulations at surface. (a) Difference in wind speed at 10 m, ΔU_{10m}, WFP-NWF; (b) Difference in TKE at 10 m, ΔTKE_{10m}, WFP-NWF; (c) Difference in significant wave height, ΔH_S, WFP-NWF. The longitude of each flight, and the corresponding flight number are printed in the title of the first row figures, as in Fig. 4.

the center of Fig. 8a, surrounded by three chosen points to be studied: P1 (6.595° E, 54.009° N), P2 (6.810° E, 54.030° N) and P3 (6.994° E, 54.049° N). During Case-2, the wind direction was from about 250°. As a result, the wind and wave fields over N3 are rather homogeneous, without gradients caused by fetch, see the spatial distribution of wind speed and H_S in Fig. 8a and b, respectively. In the absence of wind farms, the wave spectra are almost identical, supporting the conclusion that there is no obvious fetch effect on the wave field (Fig. 9a).

3.3. At the surface: do wakes enhance or weaken waves?

3.3.1. Case-1

There is no evidence from B2021 that the waves are enhanced by the presence of wind farm wake effect downwind of N4. However, such enhanced waves can be present in the simulation, in connection with WFP and the use of α. Figs. 4 and 5, through data along the flight legs, suggest a positive correlation between the surface flow acceleration (and hence enhanced waves) and the excessive TKE transported from the hub height to the surface, particularly when using $\alpha = 1$.

We examine the spatial distribution of change in U_{10m} and H_S between simulations with and without wind farm over N4 and the downwind area. The data from 14:30 UTC are shown in Fig. 7. While there are areas that are clearly under the wake effects in each subplot, the most striking feature of Fig. 7 is where $\alpha = 1$ was used (subplots a and e). By then, there is an area with accelerated surface wind and enhanced wave height, both over and shortly downwind of the farms. The overall patterns in U_{10m} and H_S are however similar for $\alpha = 0.25$, 0.1 and 0. There is a corner in Fig. 7b (with $\alpha = 0.25$) where ΔU_{10m} is also positive, though only slightly.

The grid points on the three transects A, B and C from Fig. 1 are marked in Fig. 7. In contrast to Fig. 6 where transect-B and C are compared for accessing the wake effect, here we calculate the relative wave energy change between simulation with and without wind farms along the transect-B. The results are shown in Fig. 10 for the four α values. Earlier, Fig. 6b, d, and f show the differences between transects B and C, $(S_B - S_C)/S_C$, and that the reduction of wave energy in the no-wind-farm condition is concentrated in the narrow frequency range around the peak frequency. Compared to Fig. 6, Fig. 10 shows the differences directly using $(S_{WF} - S_{NWF})/S_{NWF}$, which are clearly more similar to Fig. 6d (modeled with WFP) and Fig. 6f than Fig. 6b (modeled without WFP), with a clear dependence on the distance from N4. Compared to Fig. 6b, both Fig. 6d and Fig. 10 show a broader frequency range where significant ΔS are present. For the tracks with the most dominant wake effects (Flight Leg 4, 5 and 6), the largest wave energy reduction occurs at a frequency around 2 rad s^{-1}. Along the closest downwind Leg 2 to 4, with distance 2 km and 5 km from N4, respectively, using $\alpha = 1$ results in increased wave energy in some frequency ranges, leading to enhanced H_S over and downwind of the wind farms.

The wake-caused change in H_S is displayed in Fig. 11 as a function of longitude at 13:30, 14:30 and 15:30 UTC, covering the flight duration. Note that from 13:30 to 15:30 UTC, the wind speed has increased by 2 m s^{-1}, and accordingly the magnitude of ΔH_S also increased, with the maximum value on the transect changed from −0.02 to about −0.08 m. The largest reduction is a bit distant from N4, as a result of both horizontal and vertical propagation from hub height; this will be discussed in Section 3.4. The distribution of the change in the wave spectra with frequency is however quite similar for $\alpha = 0.25$, 0.1 and 0. Such a similarity is true for H_S as a function of the longitude.

3.3.2. Case-2

For the long-fetch Case-2, Fig. 12a and b show an example of the wind speeds and TKE at flight heights along the south-north flight legs

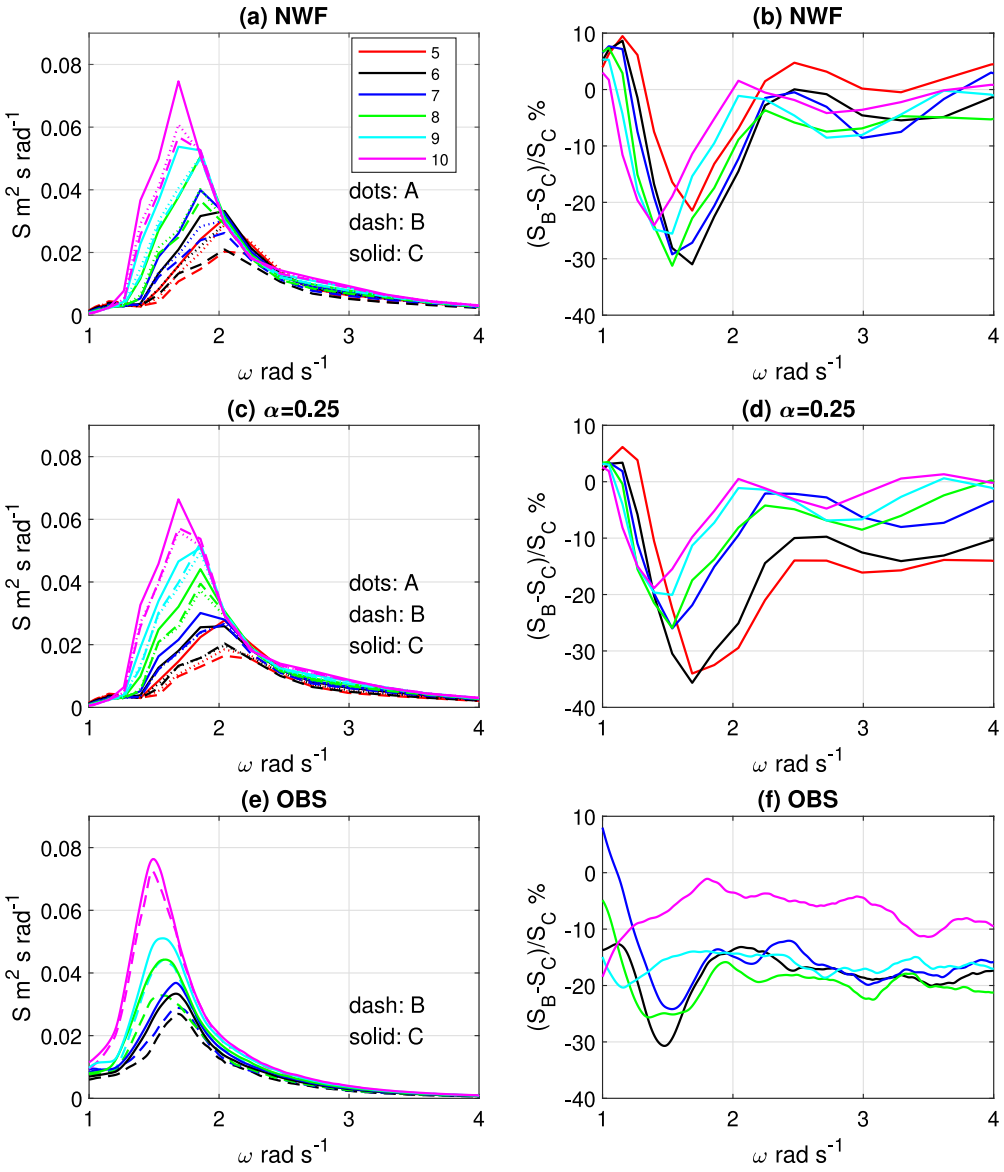

Fig. 6. Case-1. Wave spectra at points on transect-A (dotted), B (dashed) and C (solid) as defined in Fig. 1, with flight legs (with number) in different colors: showing the effect of fetch and wake. This is to compare with the method applied in B2021 for assessing the wake effect. (a) NWF; (b) NWF: Spectrum difference between transect-B and C; (c) $\alpha = 0.25$; (d) $\alpha = 0.25$: Spectrum difference between transect-B and C; (e) Measurements from B2021 (not including Flight Leg 5); (f) Spectrum difference between transect-B and C, measurements, from B2021.

over the Godewind1 wind farm from 14:30 UTC on 14 Oct. 2017, similar to Fig. 10 from LF2021. The values for $\alpha = 1$ and 0.25 are similar to those in LF2021, suggesting minor effects contributed by waves at this height in the simulation. The magnitudes of U_{HH} and TKE_{HH} are best captured by $\alpha = 1$, followed by $\alpha = 0.25$, 0.1 and 0, corresponding to smaller and smaller wake effects.

The spatial distributions of ΔU_{10} with $\alpha = 1$ and 0.25 are shown in Fig. 8c and e, respectively, and those of ΔH_S with $\alpha = 1$ and 0.25 are shown in Fig. 8d and f. The corresponding distributions for $\alpha = 0.1$ and 0 are similar to $\alpha = 0.25$, with a similar degree of difference to those in Fig. 7a–d, and they are not shown here. Consistent with simulations for Case-1, when $\alpha = 1$ is used, the surface wind acceleration is present in the simulated data downwind of wind farms, where surface waves are enhanced as a result.

For Case-2, we examined the 10-m wind speeds from the SAR data upwind and downwind of the wind farms (Fig. 1a from LF2021), which show reduced surface wind speed downwind of wind farms, with no flow acceleration. Fig. 12c shows such an example where the 10-m wind speed from SAR and simulations (with $\alpha = 1$ and $\alpha = 0.25$) are plotted together along the line shown in Fig. 8a. The SAR data over the wind farm area are not reliable and therefore not shown. The upwind and downwind wind speeds from the SAR are around 7.5 and 7 ms^{-1}, with an overall reduction in wind speed. The corresponding values for $\alpha = 0.25$ are around 8 and 7.3 ms^{-1}. For $\alpha = 1$, the upwind wind speed is the same as that for $\alpha = 0.25$, but downwind close to the wind farm, the wind speed is first higher than upwind speed, and then decreases with distance before recovering. This example shows that the simulated acceleration of the surface wind here is an artifact associated with the use of $\alpha = 1$.

We analyze the wave spectral behaviors at the three chosen grid points as shown in Fig. 8. Different from Case-1, here, while P1 is right downwind of the wind farms Borkum Riffgrund1, Borkum1 and 2 (Borkum) wind farms, P2 is some distance downwind, and P3 is influenced by the farm wakes from both Borkum and Godewind1. When using $\alpha = 1$, only at P1 waves are enhanced, while waves at both P2 and P3 are weakened by wakes (Fig. 9b). In addition, the effects from the wind farm wake are reflected at different frequencies at the three points (Fig. 9b). The result is considerably different when using $\alpha = 0.25$

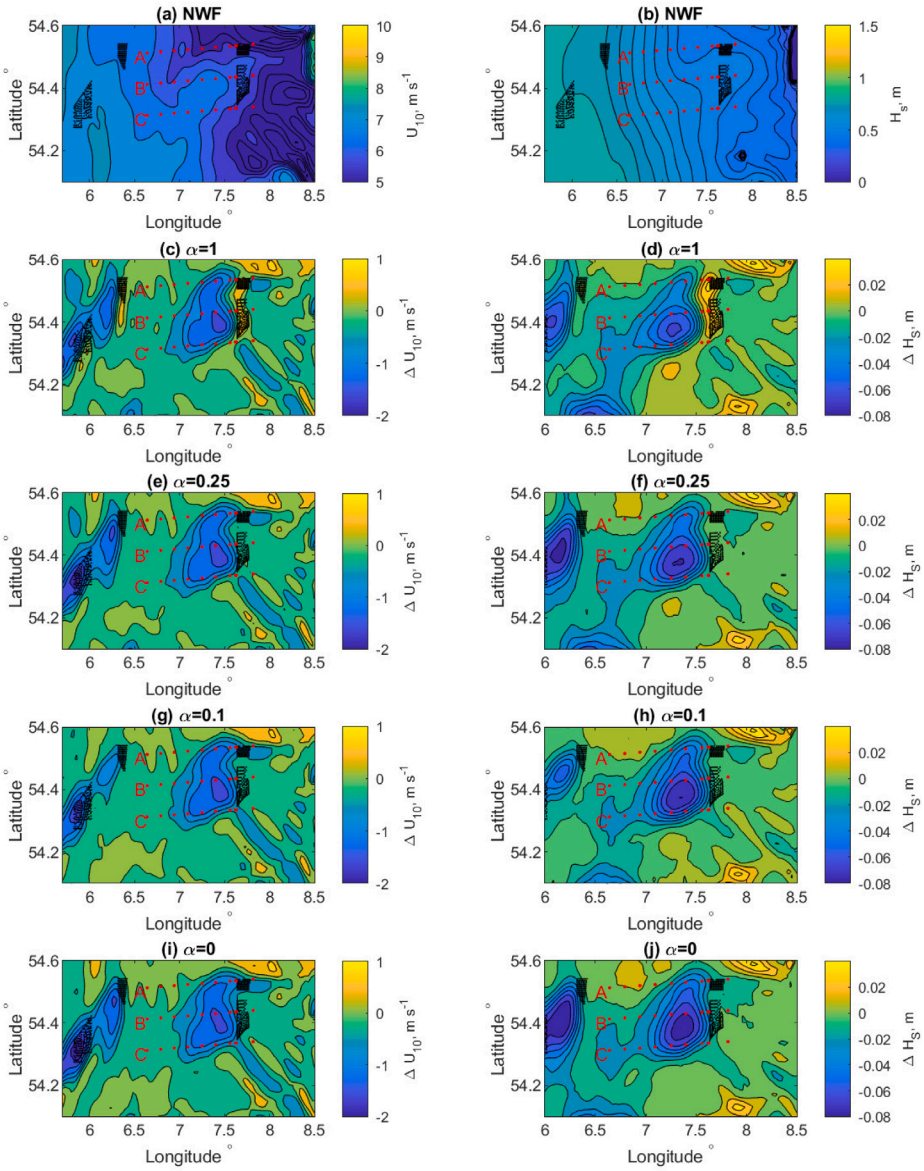

Fig. 7. Case-1. Spatial distributions of U_{10} and H_S in the absence of wind farms (a, b), $U_{10,WF} - U_{10,NWF}$ (left column) and $H_{S,WF} - H_{S,NWF}$ (right column) for 8 August 2017 at 14:30 for different values of α: Line 2 (c, d) $\alpha = 1$; Line 3 (e, f) $\alpha = 0.25$; Line 4 (g, h) $\alpha = 0.1$; Line 5 (i, j), $\alpha = 0$.

(Fig. 9c and d), where the wake effect consistently results in weakened waves, with the effect increasing from P1 to P3, as a result of wake propagation and superposition from several wind farms.

We note that the area of affected wave fields reaches a lot further downwind in Case-2 than in Case-1. It could be caused by a combined effect from atmospheric stratification and wind speed; it is a subject that deserves further investigation.

3.4. Spatial distribution on the distance-height transect

In the absence of wind farms, as surface is the source of turbulence, the momentum fluxes $< u'w' >$ and $< v'w' >$ are negative and their magnitude decreases with height in the boundary-layer. So does TKE.

Associated with the Fitch scheme, the extra source term in the presence of wind turbines (Eq. (2)) is responsible for the turbine-generated TKE, which is treated as a scalar in WRF. In WRF, the total TKE (consisting both of the wake-related TKE and non-wake related TKE) affects the magnitude of the momentum flux as shown in Eq. (3) through $q = 2 \cdot TKE$ and thus its vertical distribution from hub height to the surface. The vertical distribution of the momentum flux in turn affects if the flow accelerates or decelerates, as shown in Eq. (4). Similar analysis has been done in Fitch et al. [3] for the original study where $\alpha = 1$; they observed a positive sign of the momentum flux close to the surface, where $-\partial\overline{u'w'}/\partial z > 0$ and hence the acceleration. Here we expect to see consistent pattern of TKE and the momentum fluxes. When using smaller values of α, here 0.25 or smaller, the turbine-induced turbulence is significantly reduced to 25% or less, which, when being transported to the surface, does not usually turn the sign of the momentum flux around, and thus no flow acceleration is obtained in the calculation.

$$< u_i' u_j' >= -LqS_M \frac{\partial \overline{u_i}}{\partial z} \tag{3}$$

where $< u_i' u_j' >$ are the second-order turbulence momentum flux, which is a function of the mixing length L, stability function S_M, and

$$\frac{d\overline{u}_i}{dt} = \cdots - \frac{\partial \overline{u_i' u_j'}}{\partial x_j} + \cdots \tag{4}$$

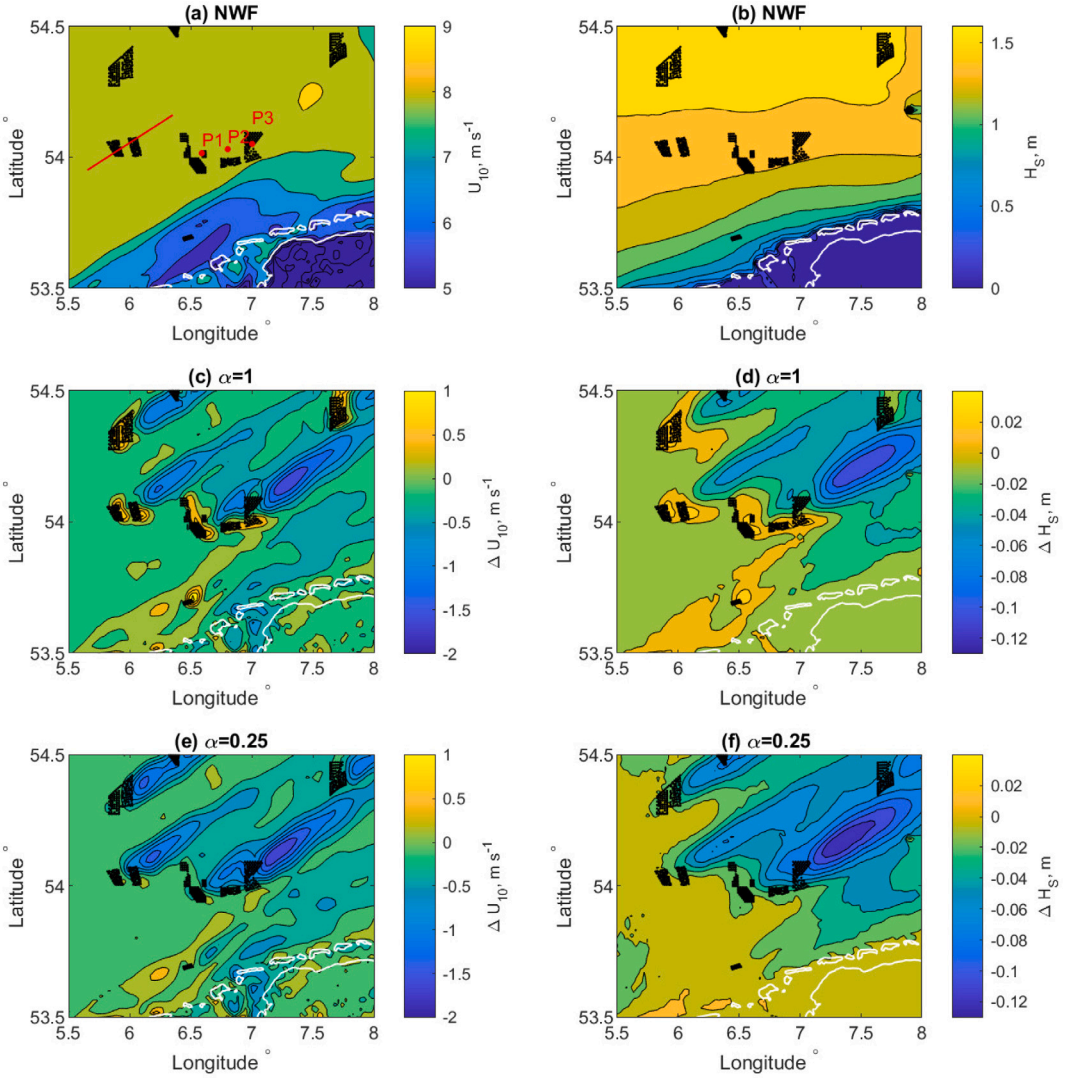

Fig. 8. Case-2. Spatial distribution of simulated (a, b) wind speed at 10 m and significant wave height with no wind farms; (c, d) deficit of wind speed $\Delta U_{10m} = U_{10,WF} - U_{10,NWF}$ and significant wave height $\Delta H_S = H_{S,WF} - H_{S,NWF}$ with $\alpha = 1$; (e, f) similar to (c, d), but with $\alpha = 0.25$. On 14 Oct. 2017, 15:00. The red line in (a) is the transect used for comparing the SAR and modeled surface wind speed.

The spatial distribution of wind speed and TKE with longitude and height provides a direct explanation to the behaviors at surface in relation to hub height, as well as upwind, over and downwind the wind farm. Figs. 13 and 14 show such an example for Case-1 at 14:30 UTC. The magnitude of ΔU at hub height between WFP and NWF is smallest when $\alpha = 1$ (3.3 ms^{-1}) and it increases with decreasing α, with the corresponding maximum value 3.5, 3.7 and 4 ms^{-1} for $\alpha = 0.25$, 0.1 and 0, respectively. Along transect-B, at the bottom of the wind farm area, only for $\alpha = 1$ an acceleration is present from the surface to about 50 m, which is marked in Fig. 13a with "> 0" (yellow area). The spread of the wind speed deficit from the hub height and from the turbines downwind results in the shift of the maximum deficit area to the west, away from the farm.

The magnitude of ΔTKE around the hub height between WFP and NWF is largest when $\alpha = 1$, and it decreases with decreasing α. This is shown in Fig. 14 for the time 14:30 UTC as an example. The corresponding maximum difference values are 1.48, 0.65, 0.44 and 0.37 m^2s^{-2} for $\alpha = 1$, 0.25, 0.1 and 0. The difference in the horizontal and vertical spatial distribution of ΔTKE caused by α values is more obvious than that of ΔU in Fig. 13. When $\alpha > 0$ (Fig. 14a–c), TKE from turbines contributed to the enhanced values over the vertical space above the wind farm, mostly concentrated in two-rotor areas above the hub height. When $\alpha = 1$, with the large value of TKE, ΔTKE is positive in the first tens of meters, which was also shown in Fig. 2. This positive ΔTKE disappeared when α is 0.25 or less. When $\alpha = 0$, when the farm-generated TKE is absent, the distribution of ΔTKE is mostly horizontal, suggesting an efficient advection of TKE from the ambient flow.

4. Discussions

We used two cases to investigate the research questions regarding how the description of the wind farm effect in the mesoscale model affects the vertical transport of turbine-generated TKE, and consequently the surface waves.

Two cases alone will not provide a full answer to these research questions; they however contribute to our understanding of the dynamics between atmosphere, waves and wind farm wakes, under different meteorological conditions and with different relations to the upwind, land effect.

Apart from their unique, respective background, another reason of revisiting the two cases is the availability of various simultaneous measurements. For the purpose of studying wakes, one obvious shortcoming of measurement data is that there is only one realization of reality, either in the presence or in the absence of wind turbines or farms. When

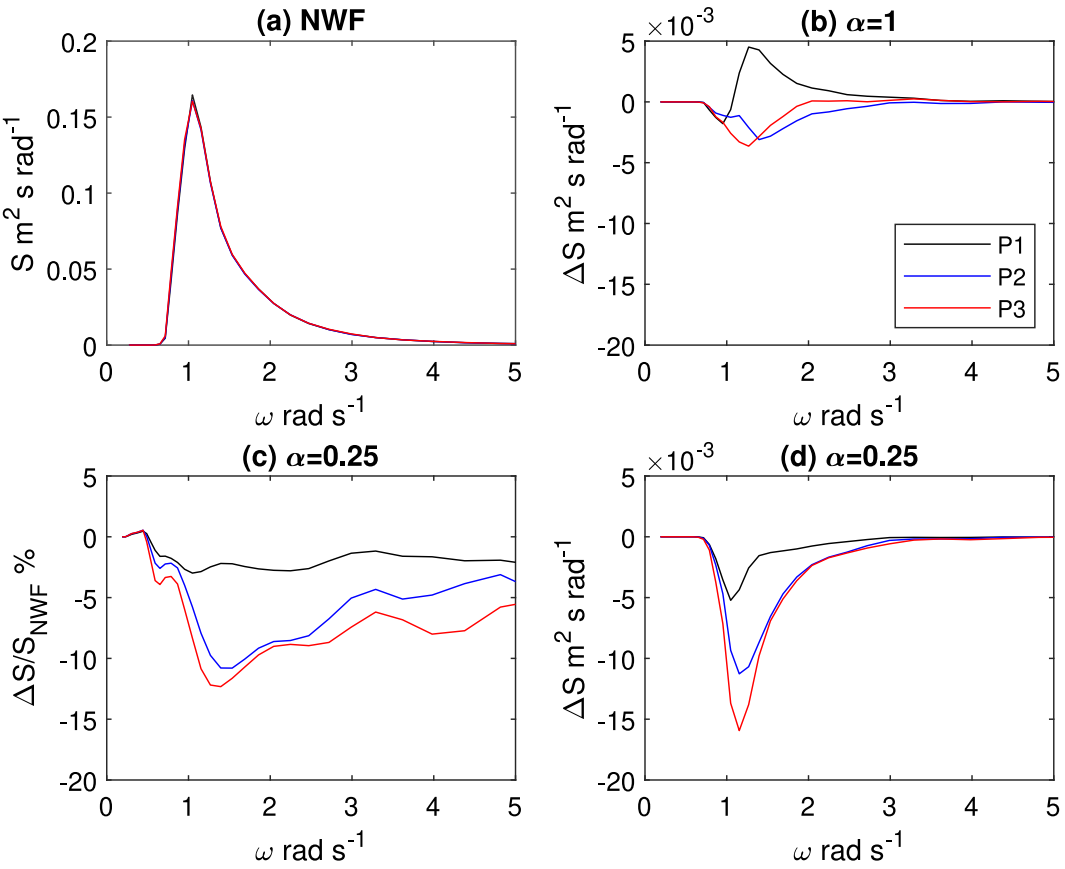

Fig. 9. Case-2. Wave spectra properties at the three points P1, P2 and P3 shown in Fig. 8 with same legends shown in subplot-(b). (a) Wave spectra as a function of radian frequency, where the spectra are the same at P1, P2 and P3; (b) Difference in wave spectra with and without wind farm, $\Delta S = S_{WFP} - S_{NWF}$ using $\alpha = 1$; (c) relative difference $\Delta S/S_{NWF}$ with $\alpha = 0.25$; (d) Difference in wave spectra with and without wind farm, $\Delta S = S_{WFP} - S_{NWF}$ using $\alpha = 0.25$.

we have only measurements, people need to be creative to "extract" information about wakes. Bodini et al. [6] and Langor [28] used measurements before and after the wind farms were in operation, and used the difference between the two periods to describe the wind farm wake effect. By doing so, one has to ignore the inter-annual variability in the measurements, which might bring considerable uncertainty in the analysis. B2021 categorize the flight data (that are continuous in time) in in- and outside of the wind farm wake region and used the difference between the two areas to describe the wake effect. By doing so, one has to assume spatial homogeneity in the background flow, which also could be a source of uncertainty in the quantification of wake effects. The SAR data that have been prepared for wake analysis often show directly the spatial distribution of surface winds close to the wind farms. The SAR images can be challenged by a few facts, too. Often an image covering wind farm clusters consists of several scenes, which can differ in time, and during this time, there is a chance the background flow may have changed. In other occasions, some images show only local winds close to the wind farms, and we might miss an overview of a larger picture of the background flow variability.

Numerical modeling provides four dimensional data describing meteorological and wave conditions continuously in time and space. It also allows the calculation of the wind farm wake effect being activated or deactivated, providing two scenarios that no measurements can. Our following-up investigation of Case-1 from B2021 demonstrates the challenges in applying measurements alone for studying wake effects; even though the signals of the wake effect are clear, it is nevertheless hard to quantify this effect. This is caused by the weakness in the assumption of spatially homogeneous background flow. Case-1 is complicated by the limited fetch effect of both atmospheric flow and wave development. The numerical modeling makes it possible to separate the wake effect from the rest.

We use a mesoscale modeling system consisting of WRF with WFP and SWAN. Such a system is limited in its ability in reproducing the sub-grid flow, including wake effects. The model provides outputs every 2 km, but only fully resolves the flow characteristics at a scale of about 14 km. Measurements are thus important and necessary for quality check of the simulations. Due to the limitations of a mesoscale model, some of the comparisons with measurements are rather qualitative. For Case-1, the model succeeded in capturing the following wake effects as suggested by the flight measurements: (1) the extension of the wake area downwind N4; (2) the reduced wind speed and enhanced turbulence in the wake area; (3) the reduced wave energy in the wake area in comparison with that outside of the wake area, with a clear dependence on the distance from N4. For Case-2, the model has demonstrated its ability in successfully capturing most of the atmospheric features shown both in LF2021 and in this paper. These provide us credibility in further analyzing the model results, with wake effects included and excluded, respectively.

Together with measurements, the modeling suggests that the observed reduction of wave energy in the frequency domain is a mixed effect from wakes, and spatial variability (partly caused by fetch effect). By comparing Fig. 6b (no wake, with spatial variability) and 6d (wake, with spatial variability), the effect of wakes can be extracted as reduced wave energy spread across the frequencies > 1 rad s^{-1}, which shows a dependence on the distance from the wind farms. This differs from the non-wake spatial variation characterized by concentrated wave energy reduction in the frequency range 1–2 rad s^{-1}, with multiple peaks at frequencies corresponding to the net wind forces from the fetch and wake effect. By removing the spatial variability, and using data with and without wakes at the same locations, Fig. 10 shows that the wake induced wave energy reduction is also across all frequencies higher

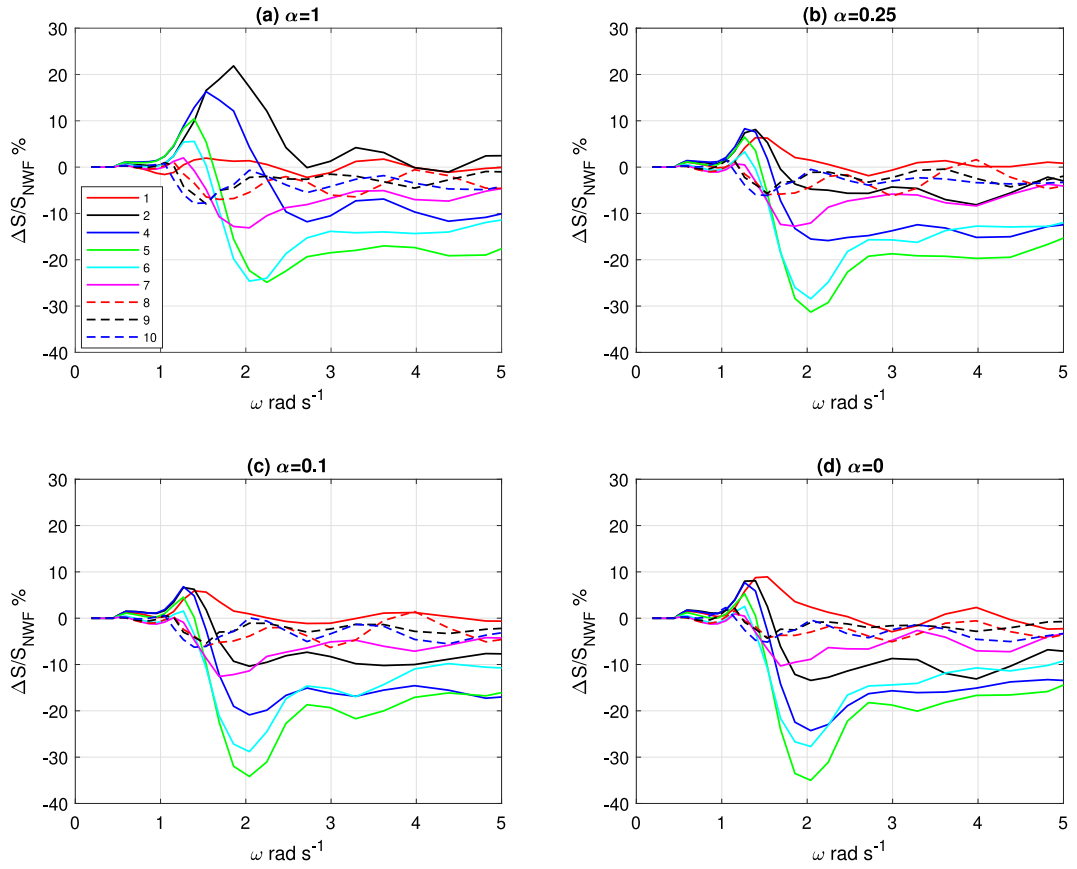

Fig. 10. Case-1. Difference in wave spectral energy in percentage $(S_{WF} - S_{NWF})/S_{NWF}$ as a function of frequency at grid points on flight legs 1–10 up- and downstream of the wind farms N4, following transect-B in Fig. 1. (a) $\alpha = 1$; (b) $\alpha = 0.25$; (c) $\alpha = 0.1$ and (d) $\alpha = 0$ at 14:30.

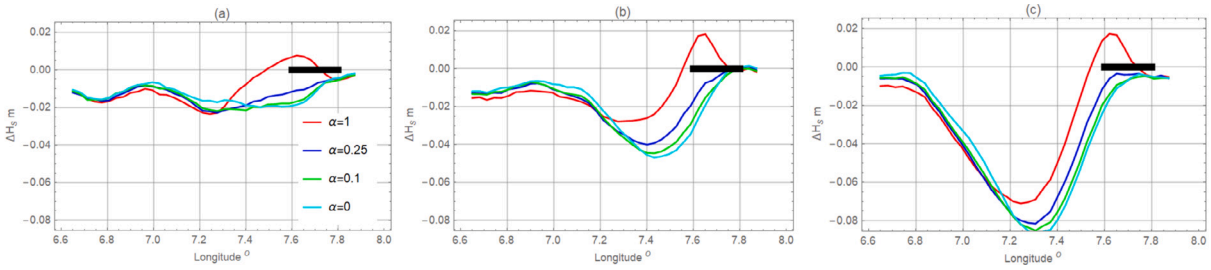

Fig. 11. Case-1. Difference in H_S between wind farms considered and not considered $(H_{S,WF} - H_{S,NWF})$, with $\alpha = 1$, 0.25, 0.1 and 0, at (a) 13:30, (b) 14:30 and (c) 15:30, along the transect-B. The thick, black line indicates approximately the location of N4.

than about 1 rad s^{-1}, with more clear peak at about 2 rad s^{-1}. Case-2 showed similar wave energy reduction across the frequency range; with stronger winds and longer fetch than case 1, the waves are stronger and more in equilibrium over the space represented by P1, P2 and P3, with the peaks more or less around 1.1 rad s^{-1}.

This study demonstrates the importance of applying numerical models to assist the analysis of measurements. Numerical modeling makes it possible to isolate the fetch effect from wake effect. B2021 did one level of separating by grouping the data in and out of the wake region. Without these processes of separating one factor from another, and without addressing the fetch effect, one may find it confusing when interpreting the increasing background flow wind speed with increasing distance from N4 as shown in Fig. 2. To acknowledge and include the fetch effect is essential for designing wind farms in the coastal zones and it remains a challenging subject for many kinds of modeling approaches, e.g., the accuracy in mesoscale numerical modeling, and the inclusion in engineering wake modeling.

Flow acceleration has been reported in numerical simulation results in connection with wind farm wake modeling. Enhanced radar scatter signals have also been reported in SAR images downwind of wind farms, which sometimes are interpreted as flow acceleration. Whereas flow acceleration on the edge of wind farms has been consistently observed, e.g. by flight [13], and SAR [29], the patterns of flow acceleration downwind of wind farms have not been shown consistently by measurements and modeling. For Case-2, SAR data do not suggest flow acceleration directly downwind of the wind farms, but the model can produce such an acceleration when we allow intensive vertical transport of TKE from hub height to the water surface by using $\alpha = 1$ in connection with the Fitch WFP scheme. For both of the two cases, whereas using $\alpha = 1$ provides best results for both reduction in wind speed and enhancement in TKE locally close to the hub height, it brought excessive TKE to the surface and introduced flow acceleration and enhanced surface waves, which are in contradiction with measurements.

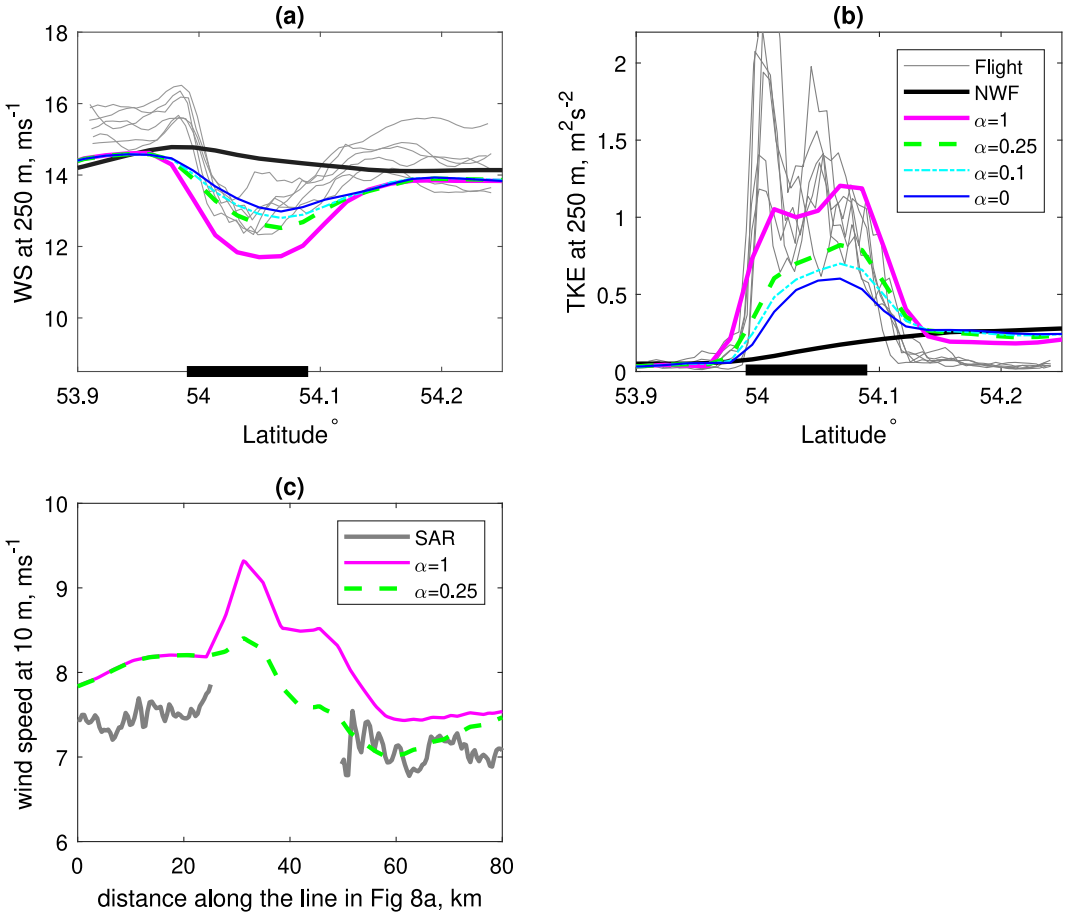

Fig. 12. Case-2. (a) Wind speed and (b) TKE at height of about 250 m above the wind farm Godewind1, measured by flights (from 15:00–17:00 UTC) and modeled (15:30 UTC) using NWF, α = 1, 0.25, 0.1 and 0. The thick black line on the x-axis shows the extend of wind farm. (c) Comparison of wind speed at 10 m between SAR (17:17 UTC) and simulations using α = 1 and 0.25 (17:20 UTC) along the line shown in Fig. 8a, from west to east.

Our study suggests using α = 1 is suitable for the analysis of wind speed and power production close to hub height, but it is not suitable for analysis at heights far from the hub height, e.g., the surface layer, and particularly for analyzing waves. Using smaller α values seems to be a more suitable choice if we are interested in lower levels, e.g. a value of 0.25. It is not easy to decide which α value to use; we tend to agree with the findings from Ali et al. (2023) that "a constant correction factor (α) is unlikely to be suitable for all scenarios". We need measurements on detailed vertical distribution of TKE under the wake effect for different meteorological conditions to help us to improve the description of the vertical transport of turbine-induced TKE from its origin.

5. Conclusions

This study demonstrates the strength of applying the fully coupled numerical modeling system in understanding the complicated mechanism of atmosphere-wave-wake interaction. It assists the analysis of measurements, which can bring difficulties in the analysis, due to their limitations in temporal and/or spatial coverage. For the subject of wakes, they can only represent one reality, either in the presence or the absence of wind farm wakes. The modeling system used here fully couples atmosphere, waves and wind farm parameterizations; it is one of the few that exist. Its capability in isolating a specific component (e.g., wakes) from other components (e.g., winds and waves), as well as combining all these components, makes it possible to decompose the complicated reality into more straightforward situations, which helps us to investigate our research questions. Cases studies are not expected to provide general answers to these research questions, they are however valuable for test and demonstrate such a model-measurement combined approach.

Through the two carefully chosen cases, it becomes clear that, for both the calculation of winds and waves relevant for offshore wind energy, more investigations are needed to understand the mechanisms and impact of the interaction between atmosphere, waves and wind farm wakes. This is partly the reason that not all validation has been quantitative, rather many of the validation have been on the conceptual, higher level, e.g., is it an acceleration or a deceleration? The numerical modeling suggests that the surface winds can accelerate in the presence of excessive turbine-generated turbulence transported to the surface layer from the hub height. This, however, did not happen in reality with the two cases, where various types of measurements suggested reduced wind speed and hence weakened waves as a result of the wind farm wake effect. The current description provides satisfactory results for hub height when α = 1 is used, but α = 1 corresponds to excessive turbine-generated TKE at the surface, causing artificial surface flow acceleration and enhanced waves. α = 0.25 is more suitable for the atmospheric surface layer and air–sea interface. This study thus shows that a more dynamic description of the advection and vertical transport of turbine-generated TKE is needed. A more systematic numerical model setup tests will be necessary, to obtain more quantitative assessment of the modeling results. For such an investigation, we also need more measurement campaigns that are designed for this purpose.

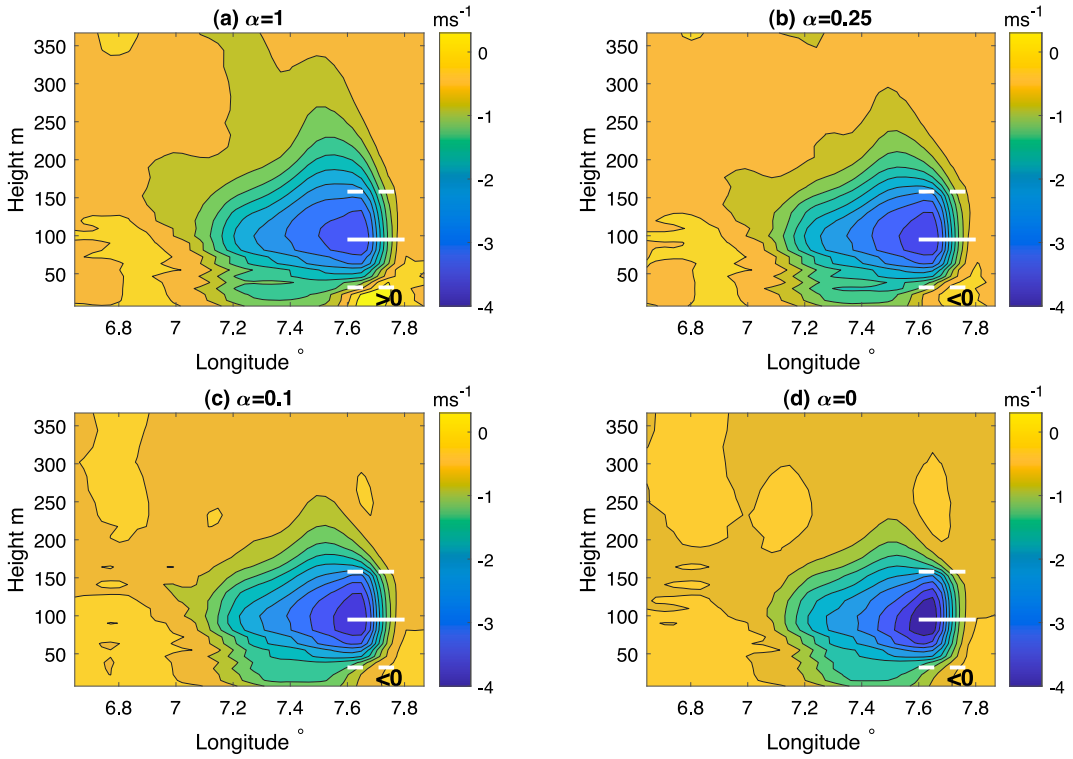

Fig. 13. Case-1. Difference in wind speed between with and without wind farms ($\Delta U = U_{WF} - U_{NWF}$), along transect-B over height up to 360 m, at 14:30. (a) α = 1 (largest deficit: −3.3 ms^{-1}); (b) α = 0.25 (largest deficit: −3.5 ms^{-1}); (c) α = 0.1 (largest deficit: −3.7 ms^{-1}); (d) α = 0 (largest deficit: −4.0 ms^{-1}). White lines suggest approximately the wind farms, with the solid line being the hub height and the dashed lines being the rotor area.

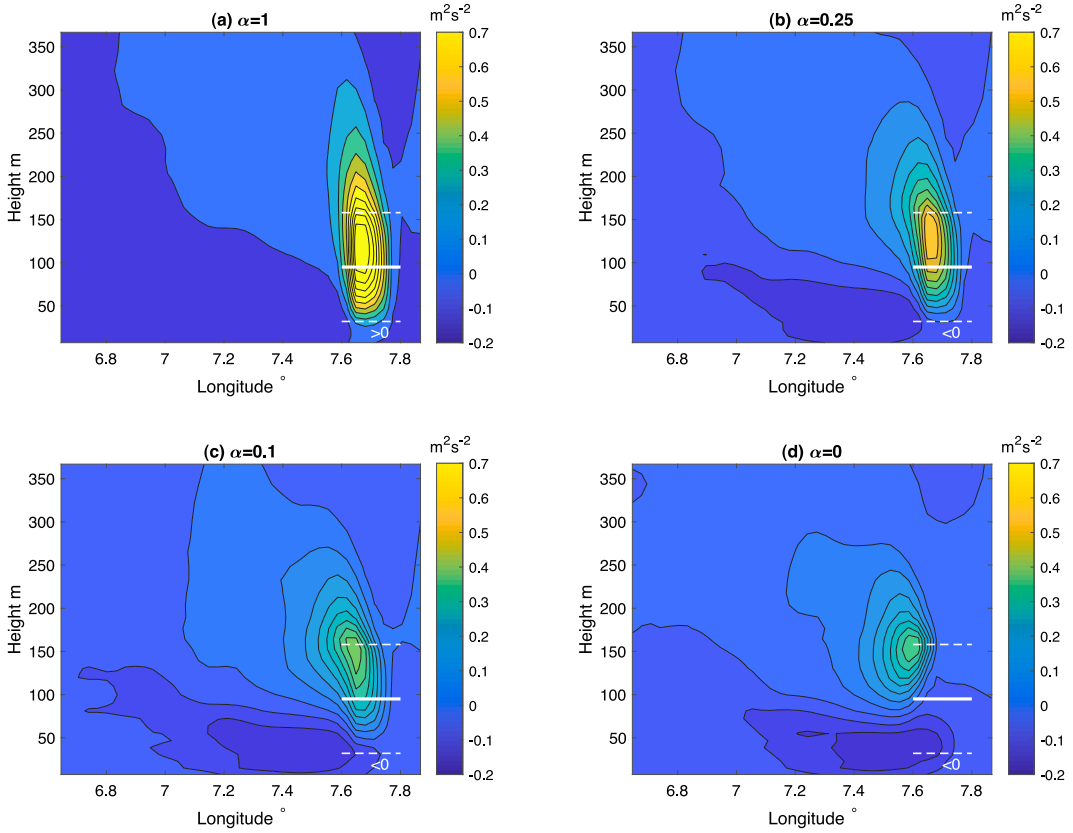

Fig. 14. Case-1. Similar to Fig. 13, but for the difference in TKE between with and without wind farms ($\Delta TKE = TKE_{WF} - TKE_{NWF}$). (a) α = 1 (largest difference: 1.48 m^{2}s^{-2}); (b) α = 0.25 (largest deficit: 0.65 m^{2}s^{-2}); (c) α = 0.1 (largest deficit: 0.44 m^{2}s^{-2}); (d) α = 0 (largest deficit: 0.37 m^{2}s^{-2}).

CRediT authorship contribution statement

Xiaoli Guo Larsén: Writing – original draft, Validation, Methodology, Formal analysis, Data curation, Conceptualization. **Jana Fischereit:** Writing – review & editing, Data curation. **Sima Hamzeloo:** Writing – review & editing. **Konrad Bärfuss:** Writing – review & editing, Data curation. **Astrid Lampert:** Writing – review & editing.

Declaration of competing interest

The authors declare that they have no known competing financial interests or personal relationships that could have appeared to influence the work reported in this paper.

Acknowledgments

We acknowledge supports from the DFF, Denmark MAMAS project (nr. 0217-00055B), Danish EUDP, Denmark project GASPOC (J. nr. 65020-1043), EU Horizon project DTWO (J. nr. 101146689).

Data availability

Data will be made available upon request. The airborne flight data is publicly available at https://doi.pangaea.de/10.1594/PANGAEA.902845 [17].

References

[1] Bughsin Djath, Johannes Schulz-Stellenfleth, Beatriz Canadillas, Impact of atmospheric stability on X-band and C-band synthetic aperture radar imagery of offshore windpark wakes, J. Renew. Sustain. Energy 10 (2018) 043301, http://dx.doi.org/10.1063/1.5020437.

[2] C. Hasager, J. Imber, J. Fischereit, A. Fujita, K. Dimitriadou, M. Badger, Wind speed-up in wind farm wakes quantified from satellite SAR and mesoscale modeling, Wind Energy 27 (2024) 1369–1387, http://dx.doi.org/10.1002/we.2943.

[3] Anna Fitch, Joseph Olson, Julie Lundquist, Jimy Dudhia, Alok Gupta, John Michalakes, Idar Barstad, Local and mesoscale impacts of wind farms as parameterized in a mesoscale NWP model, Mon. Weather Rev. 140 (2012) http://dx.doi.org/10.1175/MWR-D-11-00352.1.

[4] X. Larsén, J. Fischereit, A case study of wind farm effects using two wake parameterizations in the weather research and forecasting (WRF) model (v3.7.1) in the presence of low-level jets, Geosci. Model Dev. 14 (6) (2021) 3141–3158, http://dx.doi.org/10.5194/gmd-14-3141-2021, URL: https://gmd.copernicus.org/articles/14/3141/2021/.

[5] Cristina Archer, Sicheng Wu, Yulong ma, Pedro Jimenez, Two corrections for turbulent kinetic energy generated by wind farms in the WRF model, Mon. Weather Rev. (2020) http://dx.doi.org/10.1175/MWR-D-20-0097.

[6] N. Bodini, J. Lundquist, P. Moriarty, Wind plants can impact long-term local atmospheric conditions, Sci. Rep. 11 (2021) 22939, http://dx.doi.org/10.1038/s41598-021-02089-2.

[7] Patrick Volker, Jake Badger, Andrea Hahmann, S. Ott, The explicit wake parametrisation V1.0: A wind farm parametrization in the mesoscale model WRF, Geosci. Model Dev. 8 (2015) 3715–3731, http://dx.doi.org/10.5194/gmd-8-3715-2015.

[8] Y.T. Wu, F. Porté-Agel, Simulation of turbulent flow inside and above wind farms: Model validation and layout effects, Boundary-Layer Meteorol. 146 (2013) 108–205, http://dx.doi.org/10.1007/s10546-012-9757-y.

[9] B. Vanderwende, B. Kosovic, J. Lundquist, J. Mirocha, Simulating effects of a wind turbine array using LES and RANS, J. Adv. Modelling Earth Syst. 8 (2016) http://dx.doi.org/10.1002/2016MS000652.

[10] J. Fischereit, X. Larsén, A. Hahmann, Climatic impacts of wind-wave-wake interactions in offshore wind farms, Front. Energy Res. 10 (2022) 881459, http://dx.doi.org/10.3389/fenrg.2022.881459.

[11] S. Porchetta, D. Muñoz-Esparza, W. Munters, J. van Beeck, N. van Lipzig, Impact of ocean waves on offshore wind farm power production., Renew. Energ. 180 (2021) 1179–1193, http://dx.doi.org/10.1016/j.renene.2021.08.111.

[12] S. Porchetta, O. Temel, D. Muñoz Esparza, J. Reuder, J. Monbaliu, J. van Beeck, N. van Lipzig, A new roughness length parameterization accounting for wind-wave (mis) alignment, Atmos. Chem. Phys. 19 (2019) 6681–6700, http://dx.doi.org/10.5194/acp-19-6681-2019.

[13] A. Platis, S. Siedersleben, J. Bange, A. Lampert, K. Bärfuss, R. Hankers, B. Cañadillas, R. Foreman, J. Schulz-Stellenfleth, B. Djath, T. Neumann, S Emeis, First in situ evidence of wakes in the far field behind offshore wind farms, scientific reports, Nature Sci. Rep. (2018) http://dx.doi.org/10.1038/s41598-018-20389-y.

[14] K. Bärfuss, R. Hankers, M. Bitter, T. Feuerle, H. Schulz, T. Rausch, A. Platis, J. Bange, A. Lampert, In-situ airborne measurements of atmospheric and sea surface parameters related to offshore wind parks in the german bight, PANGAEA (2019) http://dx.doi.org/10.1594/PANGAEA.902996.

[15] M. Dörenkämper, Overview airborne measurement activities, 2021, X-Wakes Industry Workshop 8-12-2021.

[16] K. Bärfuss, J. Schulz-Stellenfleth, A. Lampert, The impact of offshore wind farms on sea state demonstrated by airborne LiDAR measurements, J. Marine Sci. Eng. (ISSN: 2077-1312) 9 (2021) http://dx.doi.org/10.3390/jmse9060644.

[17] K. Bärfuss, R. Hankers, M. Bitter, T. Feuerle, H. Schulz, T. Rausch, et al., In-situ airborne measurements of atmospheric and sea surface parameters related to offshore wind parks in the german bight, PANGAEA (2019) http://dx.doi.org/10.1594/PANGAEA.902845.

[18] A. Lampert, K. Bärfuss, A. Platis, S. Siedersleben, B. Djath, B. Cañadillas, R. Hankers, M. Bitter, T. Feuerle, H. Schulz, T. Rausch, M. Angermann, A. Schwithal, J. Bange, J. Schulz-Stellenfleth, T. Neumann, S. Emeis, In-situ airborne measurements of atmospheric and sea surface parameters related to offshore wind parks in the german bight, Earth Sys. Sci. Data 12 (2020) http://dx.doi.org/10.5194/essd-12-935-2020.

[19] J. Fischereit, H. Vedel, X. Larsén, N.E. Theeuwes, G. Giebel, E. Kaas, Modelling wind farm effects in HARMONIE–AROME (cycle 43.2.2) – part 1: Implementation and evaluation, Geosci. Model Dev. 17 (7) (2024) 2855–2875, http://dx.doi.org/10.5194/gmd-17-2855-2024, URL: https://gmd.copernicus.org/articles/17/2855/2024/.

[20] John C. Warner, Brandy Armstrong, Ruoying He, Joseph B. Zambon, Development of a coupled ocean–atmosphere–wave–sediment transport (COAWST) modeling system, Ocean Model. (ISSN: 1463-5003) 35 (3) (2010) 230–244, http://dx.doi.org/10.1016/j.ocemod.2010.07.010, URL: https://www.sciencedirect.com/science/article/pii/S1463500310001113.

[21] William C. Skamarock, Joseph B. Klemp, Jimy Dudhia, David O. Gill, Dale M. Barker, Michael G. Duda, Xiang-Yu Huang, Wei Wang, Jordan G. Powers, A Description of the Advanced Research WRF Version 3, in: NCAR Technical Notes, Technical Report 2, vol. 49, (no. 2) National Center for Atmospheric Research, Boulder, 2008, pp. 14–22, URL: https://opensky.ucar.edu/islandora/object/technotes%3A500/datastream/PDF/view.

[22] N. Booij, R.C. Ris, L.H. Holthuijsen, A third-generation wave model for coastal regions: 1. Model description and validation, J. Geophys. Res.: Oceans (ISSN: 01480227) 104 (C4) (1999) 7649–7666, http://dx.doi.org/10.1029/98JC02622.

[23] J. Du, R. Bolanos, X. Larsén, The use of a wave boundary layer model in SWAN, J. Geophys. Res.: Oceans 122 (2017) 42–62, http://dx.doi.org/10.1002/2016JC012104.

[24] J. Du, R. Bolaños, X.G. Larsén, M. Kelly, Wave boundary layer model in SWAN revisited, Ocean Sci. 15 (2) (2019) 361–377, http://dx.doi.org/10.5194/os-15-361-2019, URL: https://os.copernicus.org/articles/15/361/2019/.

[25] R. Fischereit, X. Larsén, J. Badger, G. Hawkes, Review of mesoscale wind-farm parametrizations and their applications, Bound.-Layer Meteorol. 182 (2022) http://dx.doi.org/10.1007/s10546-021-00652-y.

[26] K. Ali, D.M. Schultz, A. Revell, T. Stallard, O. Pablo, Assessment of five wind-farm parameterizations in the weather research and forecasting model: A case study of wind farms in the north sea, Mon. Weather Rev. 151 (2023) 2333–2359, http://dx.doi.org/10.1175/MWR-D-23-0006.1.

[27] D. Quint, J.K. Lundquist, N. Bodini, D. Rosencrans, Meteorological impacts of offshore wind turbines as simulated in the weather research and forecasting model, Wind Energy Sci. Discuss. 2024 (2024) 1–34, http://dx.doi.org/10.5194/wes-2024-53, URL: https://wes.copernicus.org/preprints/wes-2024-53/.

[28] E. Langor, Characteristics of offshore wind farms and their impact on wind power production from long-term modeling and measurements, 2019, DTU Wind Energy-M-0315.

[29] I. Wijnant, A. Stepek, Fit(ch) for shipping - Wind farm wake effects at 10 m height, KNMI Tech Report, 2023, https://wins50.nl/downloads/wijnantstepek2023_fitchforshipping.pdf.